# Discrete Hilbert Transform via Memristor Crossbars for Compact Biosignal Processing

Lei Zhang
Department of Electrical and Computer
Engineering
The George Washington University
Washington DC, 20052, USA
Email: zjiaz 821117@gwmail.gwu.edu

Zhuolin Yang
Department of Electrical and Computer
Engineering
The George Washington University
Washington DC, 20052, USA
Email: zlyang@gwmail.gwu.edu

Kedar Aras

Department of Biomedical Engineering
The Georgre Washington University
Washington DC, 20052, USA
Email: kedar\_aras@email.gwu.edu

Igor R. Efimov

Department of Biomedical Engineering

Northwestern University

Evanston IL, 60208, USA

Email: igor.efimov@northwestern.edu

Gina C. Adam

Department of Electrical and Computer

Engineering

The George Washington University

Washington DC, 20052, USA

Email: ginaadam@email.gwu.edu

Abstract— The Hilbert transform is widely used in biomedical signal processing and requires efficient implementation. We propose the implementation of the discrete Hilbert transform based on emerging memristor devices. It uses two matrix multiplication layers using weights programmed in the memristor array and a linear Hadamard product calculation layer mappable to CMOS. The functionality was tested on a dataset of optical cardiac signals from the human heart. The results show negligible <1% angle error between the proposed implementation and the MATLAB function. It also has robustness to non-idealities. This proposed solution can be applied to bio-signal processing at the edge.

Keywords—Hilbert Transform, Biomedical, Memristor, Inmemory Computing, Discrete Fourier Transform

## I. INTRODUCTION

Artificial intelligence algorithms and information technologies are being adopted to analyze medical data in specialties like radiology, oncology and cardiology, promising faster interpretation with accuracy close to doctors' diagnostics [1]. The next frontier is to bring these powerful algorithms to implantable medical devices. An example is the implantable cardioverter devices needed for life-saving resuscitation of patients suffering from cardiac ventricular fibrillation. Existing implantable cardioverter devices have low resolution for sensing and therapy using a single point contact sensor to estimate the heart rate. Heart conformal electronic platforms promise high spatial definition measurements across the entire heart ventricle and low-energy stimulation [2], aiming to provide personalized electrotherapy that terminates life threatening tachycardias with 10x-100x less energy than a typical shock [3]. However, the few existing prototypes used in research need a large number of wires to extract the sensor data for processing on the lab computers. In prior work [4], we have proposed a distributed analog computing algorithm which could be mapped to a network of integrated chiplets. A computing chiplet would be integrated with one or more sensors and actuators, all embedded in an organ-conformal substrate. Such system could support high resolution, ideally with hundreds or thousands of sensors for millisecond decision-making for real-time therapy. While promising, this computing technology would require the sensor signals to be pre-processed via Hilbert transform before the abnormal cardiac wavefronts can be determined.

Hilbert transform has been an important signal processing method in engineering, science, and medical applications, as it is useful to identify the dynamic characteristics of nonstationary and non-linear systems. For ventricular arrhythmias, the Hilbert transform is an efficient signal analysis method for determining the instantaneous frequency of time-varying electrocardiogram signals captured from local sensors on the heart tissue [5,6]. The Hilbert transform representation of the data is key in the detection of subtle frequency changes needed to recognize the initiation and/or termination of ventricular tachycardia / fibrillation. Therefore, an integrated real-time organ conformal system, such as the distributed network of computing chiplets previously proposed (Fig. 1), would have to include on-chip capabilities for the Hilbert transform pre-processing.

Area, energy and speed are concerns in current hardware technologies based entirely on traditional transistor CMOS circuitry [7]–[11]. Emerging electronic devices could support faster, more energy efficient and more compact implementations. Analog computing hardware based on new device technologies, such as memristors, promises to implement small neuro-inspired networks 10<sup>3</sup>-10<sup>6</sup> times faster and more efficiently than conventional technologies [12] by accelerating the vector-matrix multiplication at the physical level. Memristors (or ReRAM) are nanoscale devices with two terminals and programmable conductance which maps well to a matrix architecture (crossbar).

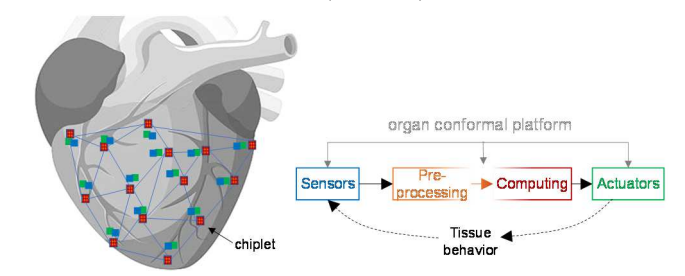


Fig.1 Motivation to implement DHT on-chiplet for pre-processing as part of a high resolution cardiac implant.

In this work, we propose the implementation of Discrete Hilbert Transform (DHT) using memristor crossbars. Since memristor devices are notorious for having device non-idealities, such as state noise, yield issues and limited precision, this work pursues an exploratory investigation via simulation that consider the potential memristor-related non-idealities and their impact on the accuracy of the memristor-

based DHT results by comparison with a software benchmark obtained in MATLAB.

#### II. METHODS

#### A. Hilbert Transform

Hilbert transform H(t) of a temporal domain signal f(t) is defined by the convolutional equation [13]:

$$H(f(t)) = -\frac{1}{\pi} \int_{-\infty}^{+\infty} f(\tau) \frac{d\tau}{\tau - t} = -\frac{1}{\pi t} * f(t) \quad (1)$$

which is a convolution between f(t) and  $-\frac{1}{\pi t}$ .

The Discrete Hilbert Transform (DHT) can be calculated based on the Discrete Fourier Transform (DFT) aiming to calculate the frequency spectrum of discrete temporal signals. The corresponding inverse process of the DFT is the inverse Discrete Fourier Transform (IDFT) to convert the frequency domain signal to the temporal domain signal. The equations are:

$$X_{k} = \frac{1}{N} \sum_{n=0}^{N-1} x_{n} e^{-jnk\left(\frac{2\pi}{N}\right)}$$
 (2)

where  $X_k$  is the discrete Fourier transform of the time domain signal  $x_n$ , n = 0, 1, 2, ..., N-1.

From the equation, the length of the time domain signal is N,  $x_n$  represents the discrete point at N. The calculated spectral value is  $X_k$ . Each  $x_n$  value at N time step is required to multiplied by the factor  $e^{-jnk\left(\frac{2\pi}{N}\right)}$ , which is a complex number. By summing up all these products, the  $k^{th}$  spectral  $X_k$  of a discrete time signal can be acquired.

$$x_n = \sum_{k=0}^{N-1} X_k e^{jnk\left(\frac{2\pi}{N}\right)} \tag{3}$$

From equation (2) and (3), the expression can be implemented via vector-matrix multiplication. Such an implementation was proposed for the Discrete Fourier Transform in [14]. The vector-matrix multiplication is implemented in digital hardware via multiply-accumulate (MAC) operations. The equation of the single MAC operation node is:

$$y = \sum_{i=1}^{m} w_i x_i \tag{4}$$

where y is the calculated output,  $x_i$  is the set of input signal with a length of i.  $w_i$  is weight matrix. As seen in Equation (4), the output is calculated via the sum of the weighted inputs. The MAC operation is critical in neural networks for artificial intelligence applications.

## B. Memristor Implementation

Emerging computing technologies, such as memristor devices, have demonstrated advantages in terms of energy and compact implementation of deep neural networks [15], mapping MAC operations physically to hardware using Ohm's and Kirchhoff's laws. They can also be ultra-scaled,

down to 2 nanometers lateral dimensions [16]. A memristor device is commonly implemented with a sandwich structure of metal-insulator-metal (Fig.2a). The intermediate insulator is typically an oxide which serves as a memristive functional material. A one-step 'forming' process is needed to create the filamentary path in the insulator. Set and reset pulses can then be reversibly applied to program the device to a desired conductance state between low (OFF) and high (ON) states (Fig.2b). Memristor devices can be integrated with complementary metal-oxide-semiconductor (CMOS) control circuitry as dense matrices (crossbars) for MAC operation (Fig.2c). A typical current-voltage characteristics of a memristor device is shown in Fig.2d.

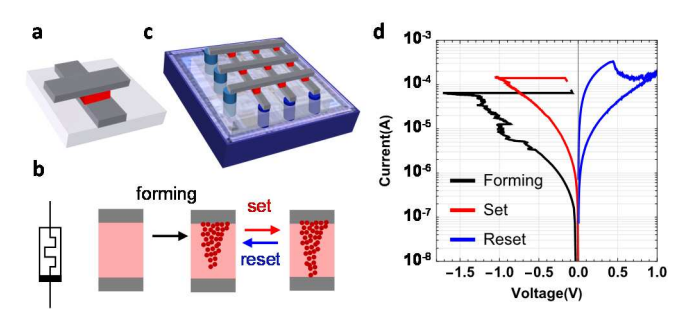


Fig.2 Memristor device. a) Structure; b) Symbol and sketch of the switching process; c) Back-end-of-line integration of a memristor crossbar (top) onto CMOS circuitry (bottom); d) Current vs. voltage characteristics.

#### C. Proposed Hilbert transform mapped to MAC operation

In this work, we propose a method of mapping Hilbert transform to the memristor-implemented MAC operations (Fig. 3). In the proposed method, the fixed weight matrices store the calculated values needed for the MAC operation to map the mathematical formula of the transformation. Each matrix supports a step in the calculation - first a fast Fourier transform, followed by an inverse fast Fourier transform. To calculate the discrete Hilbert transform, a 2-layers MAC operation structure and a linear Hadamard product layer are proposed. Both DFT and IDFT stages map the mathematical formulas to the numerical value of the memristor arrays.

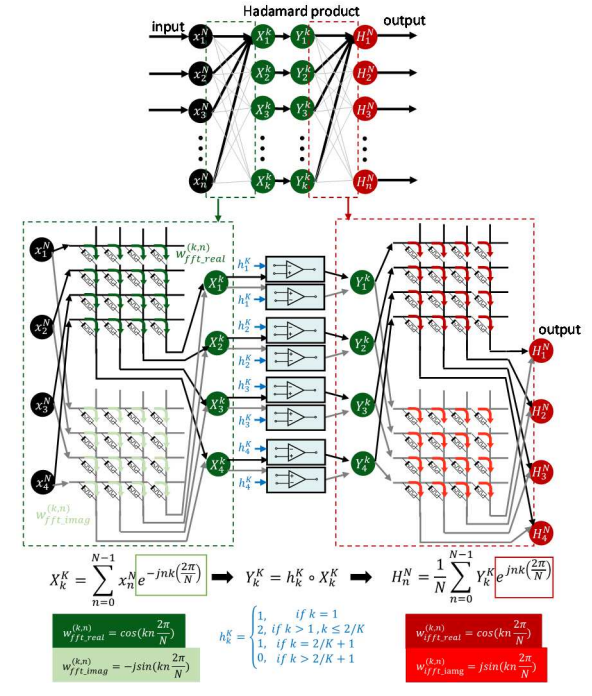


Fig.3 Sketch of the memristor-based Hilbert transform

To calculate the whole transformation, the size of the input layer needs to be equal to the sampling length of the input. For the second stage, the number of neurons in this layer depends on the length of spectral signal resulting from the DFT. These parallel nodes are necessary, and they all receive the same input values. The only difference is in their weights, the value of the weights depends on the value k, which is the index of the nodes in the second layer. A signum function connects the two to represent the convolutional term in the time domain for the Hilbert transform and zero out all negative values in the frequency domain. The third layer calculates the IDFT. All the values in the weight matrix are similar to the first layer, the only difference is the sign in the complex factor. The simulation was benchmarked against the predefined 'Hilbert' function in MATLAB.

#### D. Metrics

To compare the overall quality of the different methods, we use the root mean square error (RMSE) analysis, which is the most expressive quantity for the difference between two sets of similar samples as well as eligible for the noise performance analysis. RMSE of the memristor-based Hilbert Transform results by comparison with the benchmark MATLAB result is defined as:

$$RMSE = \sqrt{\frac{\sum_{i=1}^{N} (y_i - y_{ref_i})^2}{N}}$$
 (5)

where N is the data points in sequence of i=1,2,...,N.  $y_i$  is the actual signal need to be evaluated.  $y_{ref_i}$  is the reference of the error calculation. In this work, the reference is the MATLAB 'Hilbert' function. For both one-dimensional and two-dimensional signal, one simulation only saves one value point for the evaluation. The calculated results of the intermediate DFT are based on the spectral domain signal, and the Hilbert transform is based on the phase domain. All phase domain outputs are rescaled to the range -1 to 1 for RMSE analysis.

# III. RESULTS

#### A. Dataset

The dataset consisted of 4,000 optical maps of the fibrillation behavior in a ventricular (epicardium) tissue recorded at 1kHz sampling rate with a size of 100\*50 pixels. Optical signals were used for this study because of their high resolution of the optical signal compared to existing lower resolution electrical sensor arrays in organ conformal platforms. To obtain the data, a deidentified donor human heart from the Washington Regional Transplant Community (Falls Church, VA) was used. The study was approved by the Institutional Review Board at the George Washington University. Details on the measurement setup for this data were presented elsewhere [17].

The fibrillation events presented in the recording allow for the analysis of various wavefront patterns. An example is shown in Fig. 4. The wavefront and the singularities are detectable in phase domain, therefore, the Hilbert transform is used to transform the time domain raw optical data into the phase domain with a scale between  $-\pi$  and  $\pi$  [5].

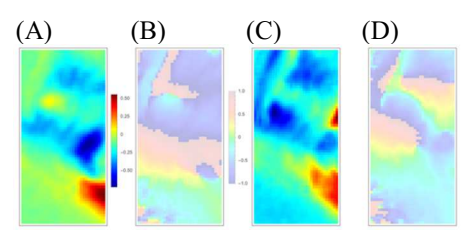


Fig.4. Representative examples of DHT on cardiac mapping. A) Raw input image #100 and B) its corresponding Hilbert transform; C-D) similar for input #150.

#### B. Ideal implementation

In this analysis, the memristor array is assumed to consist of ideal devices that have infinite resolution. Their resolution would match the MATLAB benchmark which is 64-bits floating point.

As shown in Fig.5 through the Hilbert transform, the raw input optical signal is transformed to the phase domain. Fig.5 B shows an example used for the phase domain signal of the Hilbert transform in MATLAB and the array implementation results. The RMSE is calculated on the rescaled phase domain signal where the scale is -1 to 1. These results indicate that the array implementation of the Hilbert transform can achieve a RMSE at 0.0769 on average of 4000 images compare against the benchmark.

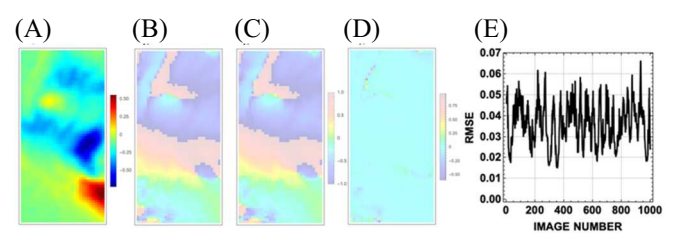


Fig.5 Proposed vs. benchmark DHT: A) an example of raw input optical signal #100; B) its benchmark phase mapping obtained from MATLAB; C) proposed DHT assuming ideal memristor crossbars; D) the difference between proposed vs. benchmark; and E) calculated RMSE for all 1000 images.

#### C. Impact of Limited Bit Precision

While the results of the RMSE analysis using the proposed method with the ideal floating-bit precision are promising, such high-level precision is not possible to achieve in hardware implementation because of the constrains of the memristor device, as well as power and area in neuromorphic hardware for inference at the edge. Memristor devices have shown to have >6-bit equivalent number of states.

In this section, the results for lower fixed-bit precision simulation are investigated, to make the algorithm easily mappable for hardware. The rounding method in this study is rounding-to-nearest. Fig.6 compared the results with the different bit level limitations. Bit level from 1 bit to 8 bit was explored. The results indicates that the overall RMSE decreases as the bit value increases. At bit level 6, possible with a memristor implementation, the averaged RMSE is 0.1579 which is very close to the ideal case. This is promising since memristor devices have shown to have >6-bit equivalent number of states [17,18].

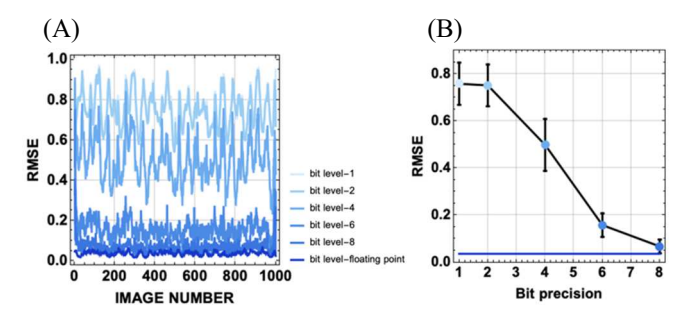


Fig.6 Bit precision analysis, A) RMSE for all images calculated for various bit precision levels vs. the 64 floating point precision from MATLAB, B) mean RMSE for different bit precision levels. Error bars represent standard deviation.

## D. Read Noise Analysis

Another concern is the reading noise which might occur when doing the MAC operation through the pre-programmed memristor array. The memristor potentially could suffer from read noise, as prior literature has shown typical noise level for oxide-based devices with a standard deviation of 0.007 to 0.1 due to Johnson-Nyquist noise, random telegraph noise, etc.[20]

The results shown in Fig.7 indicate that the performance of the algorithm in terms of RMSE are robust to read noise. The noise was modeled as a Gaussian distribution with mean equals to 0 and desired standard deviation. The noise model applied to all 4 metrics for both real and imaginary part for both FFT and IFFT. The value in the model is limited to 1 (representing the maximum conductance of the memristor) and -1 (its respective minimum conductance). With a larger standard deviation, by applying the noise model, the value of the memristor array might exceed 1 or -1, so truncation is used to clip the value. In Fig.7 (B), the worst case of RMSE is at sigma=0.1, with the value of averaged 0.2881 for all pixels through all datasets.

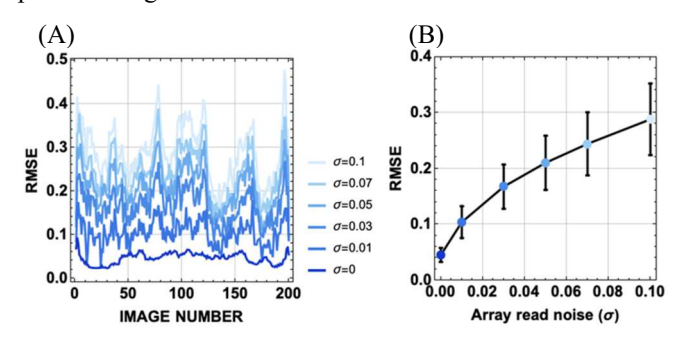


Fig.7 Read noise analysis, A) RMSE between reading noise levels (mean=0, sigma varying) and the benchmark calculated from MATLAB internal function through all images, B) averaged overall RMSE for different levels of the read noise. Error bars represent standard deviation.

#### E. Error rate

Another potential reliability issue is the device stuck error rate analysis, due to yield issues. As shown in Fig. 8 the inference of the edge computing is not robust to failed devices, either the ON or OFF state. With a 10% error rate, the RMSE increases to ~0.3. The stuck-to-ON and stuck-to-OFF states have shown to experience a similar negative impact in terms of the RMSE. This poor performance in arrays with poor yield is expected, since each of the weight in the array corresponds to a frequency in the spectral domain, which can be significant for the investigated DHT map. However, given the critical requirements for the

highest-performing components embedded in a medical implant, the average yield is not necessarily a concern since each chiplet would be individually tested, selected, and assembled in the proposed computing application for robust integration with the sensors, actuators and the rest of the computing circuitry.

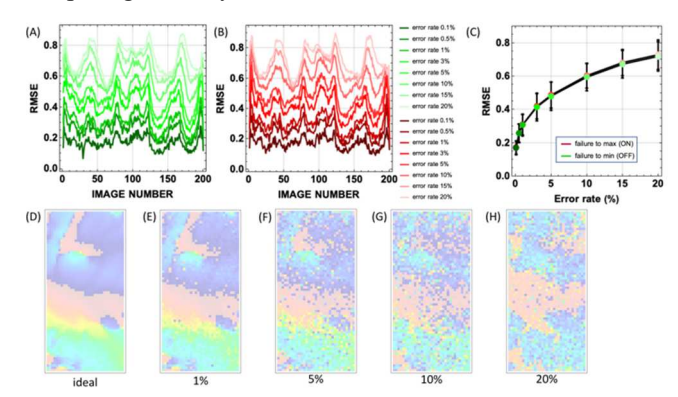


Fig. 8 Impact of device stuck error rate: A) RMSE between multiple error ratios and the benchmark calculated from MATLAB internal function through all images for failure to minimum (stuck-to-OFF); B) RMSE between multiple error ratios and the benchmark calculated from MATLAB internal function through all images for failure to maximum (stuck-to-ON); C) the averaged RMSE for each error ratios for both failure modes; D) Respective outputs for DHT considering the ideal case versus E-H) 1%, 5%, 10%, and 20% of memristor devices stuck to ON respectively.

#### IV. CONCLUSION

In this paper, we proposed a memristor-based Hilbert transform and investigated its potential for potential use with non-ideal memristor arrays for cardiac signal pre-processing. By analyzing the performance in terms of the RMSE compared against the benchmark at multiple bits precision, reading noise levels and device stuck error rates cases, the reliability of energy efficient memristor implementation of Hilbert shows promise for potential integration into chiplets for cardiac implants. Beyond the Hilbert transform for cardiac mapping, this memristor-based MAC operation structure could be investigated for other biomedical applications, for example for processing auditory and electroencephalography signals [21], [22].

## ACKNOWLEDGMENT

This work was supported by the NSF grant CRII: FET 1948127, NIH grant R01HL141470, NIH grant 1K99HL148523-01A1, Leducq Foundation grant RHYTHM, and the George Washington University Cross-Disciplinary Research Fund. All experiments were conducted on deidentified human heart tissue and approved by the Institutional Review Board (Office of Human Research) at George Washington University.

#### REFERENCES

- [1] E. J. Topol, "High-performance medicine: the convergence of human and artificial intelligence," *Nat Med*, vol. 25, no. 1, pp. 44–56, Jan. 2019, doi: 10.1038/s41591-018-0300-7.
- [2] L. Xu et al., "3D multifunctional integumentary membranes for spatiotemporal cardiac measurements and stimulation across the entire epicardium," Nat Commun, vol. 5, no. 1, p. 3329, May 2014, doi: 10.1038/ncomms4329.
- [3] S. Buchan, R. Kar, M. John, A. Post, and M. Razavi, "Electrical Stimulation for Low-Energy Termination of Cardiac Arrhythmias: a Review," *Cardiovasc Drugs Ther*, Aug. 2021, doi: 10.1007/s10557-021-07236-5.
- [4] Z. Yang, L. Zhang, K. Aras, I. R. Efimov, and G. C. Adam, "Hardware-Mappable Cellular Neural Networks for Distributed Wavefront

- Detection in Next-Generation Cardiac Implants," *Advanced Intelligent Systems*, p. 2200032, May 2022, doi: 10.1002/aisy.202200032.
- [5] S. R. Gutbrod et al., "Quantification of the Transmural Dynamics of Atrial Fibrillation by Simultaneous Endocardial and Epicardial Optical Mapping in an Acute Sheep Model," Circ: Arrhythmia and Electrophysiology, vol. 8, no. 2, pp. 456–465, Apr. 2015, doi: 10.1161/CIRCEP.114.002545.
- [6] M. P. Nash et al., "Evidence for Multiple Mechanisms in Human Ventricular Fibrillation," Circulation, vol. 114, no. 6, pp. 536–542, Aug. 2006, doi: 10.1161/CIRCULATIONAHA.105.602870.
- [7] M. B. Pawloski, X. Tang, J. Harley, K. Bi, T. Özdemir, and S. Mandal, "Sparse sensor networks for active structural health monitoring using highly integrated CMOS transceivers," in Sensors and Smart Structures Technologies for Civil, Mechanical, and Aerospace Systems 2018, Denver, United States, Mar. 2018, p. 129. doi: 10.1117/12.2296664.
- [8] N.-F. Chang, T.-C. Chen, C.-Y. Chiang, and L.-G. Chen, "On-line empirical mode decomposition biomedical microprocessor for Hilbert Huang transform," in 2011 IEEE Biomedical Circuits and Systems Conference (BioCAS), Nov. 2011, pp. 420–423. doi: 10.1109/BioCAS.2011.6107817.
- [9] P. S. Reddy, S. Mopuri, and A. Acharyya, "A Reconfigurable High Speed Architecture Design for Discrete Hilbert Transform," *IEEE Signal Process. Lett.*, vol. 21, no. 11, pp. 1413–1417, Nov. 2014, doi: 10.1109/LSP.2014.2333745.
- [10] L. Liu and Y. Zhang, "Design and Implementation of Reconfigurable Discrete Hilbert Transform Based on Systolic-Arrays," in 2010 International Conference on Communications and Mobile Computing, Shenzhen, China, Apr. 2010, pp. 245–249. doi: 10.1109/CMC.2010.136.
- [11] A. Prince, P. Verma, C. Jayakumar, and D. Raju, "Efficient architecture for real time implementation of Hilbert Transform in FPGA," 2015 IEEE International Conference on Electrical, Computer and Communication Technologies (ICECCT), 2015, doi: 10.1109/ICECCT.2015.7226158.
- [12] L. Ceze et al., "Nanoelectronic neurocomputing: Status and prospects," in 2016 74th Annual Device Research Conference (DRC), Jun. 2016, pp. 1–2. doi: 10.1109/DRC.2016.7548506.

- [13] V. Cizek, "Discrete Hilbert transform," *IEEE Trans. Audio Electroacoust.*, vol. 18, no. 4, pp. 340–343, Dec. 1970, doi: 10.1109/TAU.1970.1162139.
- [14] R. Velik, "Discrete Fourier Transform Computation Using Neural Networks," in 2008 International Conference on Computational Intelligence and Security, Dec. 2008, vol. 1, pp. 120–123. doi: 10.1109/CIS.2008.36.
- [15] D. Ielmini and H.-S. P. Wong, "In-memory computing with resistive switching devices," *Nat Electron*, vol. 1, no. 6, pp. 333–343, Jun. 2018, doi: 10.1038/s41928-018-0092-2.
- [16] S. Pi et al., "Memristor crossbar arrays with 6-nm half-pitch and 2-nm critical dimension," *Nature Nanotech*, vol. 14, no. 1, pp. 35–39, Jan. 2019, doi: 10.1038/s41565-018-0302-0.
- [17] K. K. Aras, N. R. Faye, B. Cathey, and I. R. Efimov, "Critical Volume of Human Myocardium Necessary to Maintain Ventricular Fibrillation," Circ: Arrhythmia and Electrophysiology, vol. 11, no. 11, Nov. 2018, doi: 10.1161/CIRCEP.118.006692.
- [18] C. Li et al., "Analogue signal and image processing with large memristor crossbars," Nat Electron, vol. 1, no. 1, pp. 52–59, Jan. 2018, doi: 10.1038/s41928-017-0002-z.
- [19] Z. Wang et al., "Resistive switching materials for information processing," Nat Rev Mater, vol. 5, no. 3, pp. 173–195, Mar. 2020, doi: 10.1038/s41578-019-0159-3.
- [20] M. Zhao, B. Gao, J. Tang, H. Qian, and H. Wu, "Reliability of analog resistive switching memory for neuromorphic computing," *Applied Physics Reviews*, vol. 7, no. 1, p. 011301, Mar. 2020, doi: 10.1063/1.5124915.
- [21] O. Etard, M. Kegler, C. Braiman, A. E. Forte, and T. Reichenbach, "Decoding of selective attention to continuous speech from the human auditory brainstem response," *NeuroImage*, vol. 200, pp. 1–11, Oct. 2019, doi: 10.1016/j.neuroimage.2019.06.029.
- [22] R. J. Oweis and E. W. Abdulhay, "Seizure classification in EEG signals utilizing Hilbert-Huang transform," *BioMed Eng OnLine*, vol. 10, no. 1, p. 38, May 2011, doi: 10.1186/1475-925X-10-38.